Coinage Metal−Sulfur Complexes: Stability on Metal(111) Surfaces and in the Gas Phase

Jiyoung Lee,[†,‡] Theresa L. Windus,[†,‡] Patricia A. Thiel,[†,‡,§] James W. Evans,[†,∥] and Da-Jiang Liu*[,†]

[†]Ames Laboratory−USDOE, [‡]Department of Chemistry, [§]Department of Materials Science & Engineering, and [∥]Department of Physics and Astronomy, Iowa State University, Ames, Iowa 50011, United States

*Supporting Information

ABSTRACT: We provide a comprehensive theoretical assessment at the level of density functional theory (DFT) of the stability of various coinage metal−sulfur complexes, both in the gas phase and also for the complexes adsorbed on the (111) surface of the same coinage metal. Our primary interest lies in the latter where earlier scanning tunneling microscopy (STM) experiments were interpreted to suggest the existence of adsorbed S-decorated metal trimers, sometimes as a component of more complex adlayer structures. Recent STM studies at 5 K directly observed other isolated adsorbed metal−sulfur complexes. For these adsorbed species, we calculate various aspects of their energetics including a natural measure of stability corresponding to their formation energy from sulfur adsorbed on terraces and from metal atoms that are in thermal equilibrium with the substrate. From this perspective, our DFT analysis shows that all of Ag_2S_3, Ag_3S_3, and many larger complexes on Ag(111) are strongly stable, Cu_2S_3 is stable, and some larger complexes are marginally stable on Cu(111), but only Au_4S_4 on Au(111) is stable. Results are consistent with STM observations for Cu(111) and Ag(111) surfaces but appear to deviate slightly for Au(111). A systematic analysis relating stability in the gas phase with that of adsorbed species is achieved within the framework of Hess's law. This analysis also unambiguously elucidates various energetic contributions to stability.

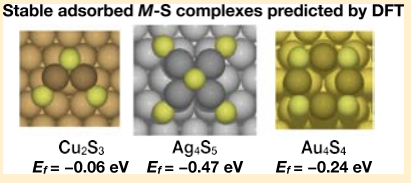

1. INTRODUCTION

Over the last decade, there have been several observations from scanning tunneling microscopy (STM) analysis of small stable metal (M)−chalcogenide complexes, and in particular, M−S complexes, adsorbed on hexagonal close-packed (111) surfaces of the same or different metals. Perhaps the most definitive observation is from STM at 5 K of heart-shaped Cu_2S_3 complexes on Cu(111).[1] In addition, adlayer clusters formed after exposure of Ni(111) to H_2S were proposed to be composed of Ni_3S_3 complexes,[2] and massive S-induced transformation of nanometer-sized Co nanoparticles on Au(111) was found to be mediated exclusively by the formation and detachment of Co_3S_4 complexes.[3] More speculative STM studies suggested the presence of Au_3S_3 complexes after adsorption of S on Au(111) at liquid nitrogen temperatures[4] and of Cu_3S_3 complexes as a component of intricate adlayer structures near step edges on Cu(111) observed down to 50 K.[5] However, the latter interpretation was not supported by more recent studies at 5 K.[6] In some cases, significantly larger complexes were also observed at 5 K with a linear "polymeric" structure: $Ag_{n+1}S_n$ and $Ag_{13n+3}S_{9n+4}$ for $n > 1$ on Ag(111)[7] and $Cu_{16}S_{13}$ for $n > 2$ on Cu(111).[6] Beyond the observed structures, other small complexes have been suggested to occur as stable absorbed moieties: MS_2, MS_3, M_3S_3, and so forth on M(111) for coinage metals M = Cu and Ag.[1,8,9] The smaller complexes have been implicated as carriers in dramatically enhanced metal mass transport observed on some surfaces, for example, in the form of accelerated decay of smaller two-dimensional (2D) metal nanoclusters.[1,8−11] Such enhancement can occur in the presence of even trace amounts of chalcogen.

Still considering metal (M)−chalcogen systems, we note that M−O complexes have long been speculated to play a role in the degradation through coarsening of supported catalyst nanoparticles, particularly PtO_2 for supported Pt nanoparticles.[12−14] Degradation might occur via transport either across the surface or through the gas phase. Also, Ag−O complexes have been suggested to play a role in surface mass transport on Ag(100) surfaces.[11,15] With regard to other classes of systems, M−hydrogen,[16,17] M−halide,[18−20] and M−CO[21−23] complexes have all been considered. In fact, long ago it was proposed that formation of mobile adsorbate−metal complexes might occur whenever electronegative adsorbates interact with "soft" metals.[19] Also of relevance is that various M−halide and M−chalcogenide molecules in the gas phase are found to be end products of dry etching processes.[24] Finally, we mention that X−Au−X complexes with X = alkylthiolate have been proposed to play a role in molecular self-assembly on Au surfaces. These have been observed directly in the case of X = CH_3S[25] for which stability has been confirmed by density functional theory (DFT) analysis.[26]

However, what has been lacking is a comprehensive theoretical exploration of the stability of these various adsorbed complexes. This exploration might naturally compare at least trends in stability for adsorbed complexes with those in

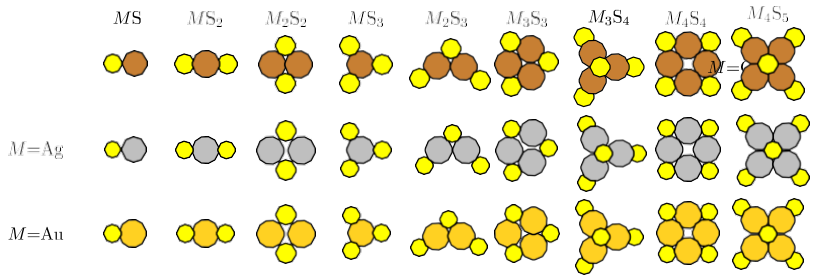

Figure 1. Geometries of gas-phase M_mS_n complexes based on PBE predictions. Light yellow circles denote S atoms, with diameter selected as the bond length of S_2. Brown, gray, and dark yellow denote Cu, Ag, and Au atoms, respectively, where diameters are selected to match the nearest-neighbor distance in the bulk metal. Configurations for M_mS_n(gas) for different M are quite similar with only slight differences in bond lengths and angles. MS_2 are linear; M_2S_2, MS_3, M_2S_3, M_3S_3, and M_4S_4 are planar.

the gas phase. In fact, the latter comparison can be made systematic within the framework of Hess's law. We pursue this goal here for M−S complexes on the low-index M(111) surface of the same coinage metal for M = Cu, Ag, or Au. We have previously studied M_3S_3 complexes and assess whether it is reasonable to assign experimentally observed features on the metal surface exposed to sulfur to this particular complex.[26] In this work, we greatly expand consideration to a set of nine distinct complexes for each of three different coinage metals. Comparison with previous analysis is made.

The contents of the paper are as follows. The methodology for our DFT-based analysis is described in Section 2. Although our primary interest and focus are on adsorbed complexes, results for calculations of gas-phase stability are first presented in Section 3, as these will be utilized in subsequent analysis. Next, results for adsorbed M−S complexes are presented in Section 4. Section 5 relates the stabilities of adsorbed complexes with the gas-phase energetics within the framework of Hess's law, as mentioned above. Concluding remarks are given in Section 6.

2. METHODOLOGY

DFT calculations are generally carried out using two different types of basis sets. For extended and periodic systems, it is most natural to use a plane-wave (PW) basis set. For such analyses, in this paper, we use the VASP package (v5.4)[27,28] and the standard PAW potentials[29,30] that are included in the package. The Perdew−Burke−Ernzerhof (PBE)[31] functional is used for slab calculations probing the energetics of adsorbed complexes. In these calculations, the surface is represented by a periodic array of slabs, separated by 1.2 nm of vacuum. Lattice constants for the face-centered cubic metal substrates are taken as theoretical values obtained with the energy cutoff of 280 eV for the PBE functional. S and M−S complexes are adsorbed on top of each slab (rather than on both sides). The total energy of the system is then minimized allowing both the adsorbate and metal substrate or slab atoms to relax, except for the bottom layer of the slab. The convergence criterion requires that all forces are below 0.02 eV/Å. All surface energetics are obtained from averages over 4−7 layer slabs, which have the effect of minimizing quantum size effects associated with electron confinement in thin slabs. Most calculations involving adsorbed complexes are carried out with (4 × 4) lateral supercells.

For analysis of gas-phase energetics, we also somewhat unconventionally calculate energetics using the same PW basis set, which allows consistent comparison with the analysis of adsorbed complexes. Gas-phase complexes are simulated using three-dimensional orthogonal periodic cells. In addition to the PBE functional used extensively for surface calculations, the hybrid PBE0,[32] meta-GGA SCAN,[33] and optB88-vdW[34,35] functionals are used for the gas-phase analyses. These PW results are compared with the local basis calculations described below, thereby facilitating the validation of both approaches.

Because the PW DFT calculations involve different bulk, surface, and gas phases, different choices of smearing of the electron occupancy are needed. For bulk, we use the tetrahedron method with Blöchl corrections.[36] For gas-phase forms of individual atoms, diatomic S_2, and complexes, Gaussian smearing of width 0.002 eV is used. For surface calculations, the first-order Methfessel−Paxton smearing of width 0.2 eV is used. Nonspin-polarized DFT is used for bulk and slab calculations, and spin-polarized DFT is used for atoms and complexes in the gas phase. For each supercell, we use a *k*-point mesh that is closest to the equivalent of (24 × 24 × 1) for the unit surface cell. Selected calculations with spin-polarized DFT adsorbed complexes show that the ground states of Cu, Ag, and Au slabs with adsorbed S or metal−sulfur complexes have no magnetic moment.

For gas-phase atoms and complexes, atomic or Gaussian-type orbitals (GTOs) constitute more natural basis sets. Thus, DFT calculations with GTO basis sets are performed with the NWChem software.[37] All structures are optimized to minimize energy with PBE[31] and PBE0[32] functionals using three different basis sets. For the smallest basis set, we use Los Alamos National Laboratory Double Zeta (LANL2DZ) with effective core potentials (ECPs)[38−40] for metals and 6-311++G(d,p)[41−43] for S. It is denoted by DZ/TZ. For two larger basis sets, we use def2-NZVP for metals[44,45] (small ECP is used for heavier atoms, Ag and Au) and def2-NZVPPD for S[46] (N = T, Q). They are denoted by TZ/TZ and QZ/QZ, respectively. Spherical functions are used for N = Q to eliminate linear dependence problems. To find minimum energy states, initial M_nS_m complexes are optimized at different possible spin multiplicities using DZ/TZ basis sets. For instance, if the number of metals is even (odd), multiplicities such as doublet, quartet, sextet, and so forth (singlet, triplet, quintet, etc.) are explored and the spin state with the lowest energy is chosen. Some of our analysis will require energies, $E[M_m(\text{gas})]$, for metal clusters in the gas phase, for which we use a similar approach. For the S atom, the triplet state is used. After the spin states are determined, complexes are optimized with the smallest basis sets DZ/TZ first and reoptimized later with larger basis sets. Restricted open-shell DFT (RODFT) is used for open-shell systems with the number of radial grid

Table 1. Atomization Energy E_a(Gas) (in Electronvolt) of the Gas-Phase M_mS_n Complex, Obtained Using the VASP Code[a]

	MS	MS_2	M_2S_2	MS_3	M_2S_3	M_3S_3	M_3S_4	M_4S_4	M_4S_5
					PBE				
Cu	3.23	5.82	10.02	7.75	11.87	16.63	17.34	23.06	22.41
Ag	2.46	4.52	7.44	5.79	9.06	12.69	13.32	17.49	17.34
Au	2.94	5.92	8.49	7.51	11.51	14.92	16.41	21.60	20.87
					PBE0				
Cu	2.92	5.18	8.99	6.17	10.52	15.04	15.47	20.47	20.06
Ag	2.29	3.87	6.70	4.25	8.00	11.82	11.57	16.46	15.87
Au	2.62	5.18	7.68		10.08	13.56	14.41	19.48	18.71
					SCAN				
Cu	3.16	5.34	9.95	7.54	11.80	16.77	17.43	23.41	22.74
Ag	2.34	4.40	7.16	5.39	8.86	12.75	13.19	17.65	17.27
Au	3.05	6.01	8.67		12.07	15.84	17.28	22.96	22.26
					optB88-vdW				
Cu	3.20	5.82	9.88	7.72	11.72	16.46	17.20	22.80	22.33
Ag	2.47	4.52	7.52	5.91	9.10	12.79	13.44	17.76	17.62
Au	2.95	5.95	8.56	7.60	11.52	15.04	16.54	21.75	21.08

[a]Missing values correspond to unstable complexes.

points and angular points in the Lebedev grid being chosen as 99 and 590, respectively.

3. ENERGETICS OF GAS-PHASE COMPLEXES

The list of metal−sulfur complexes considered here is motivated by their existence (either proposed or confirmed) on (111) surfaces and also by their anticipated stability in the gas phase. However, we exclude those configurations that include S−S bonds because we are mostly concerned with low S coverages for surface systems where it is generally more energetically favorable for disulfur to dissociate and to bond with metal atoms. Figure 1 shows the nine types of M_mS_n complexes, MS, MS_2, M_2S_2, MS_3, M_2S_3, M_3S_3, M_3S_4, M_4S_4, and M_4S_5, which we analyze. Geometries shown are optimized using the PBE functional and the VASP code.

3.1. Atomization and Formation Energies. The atomization energy of the M_mS_n complex in the gas phase is defined as

$$E_a(M_mS_n)(\text{gas}) = mE[M(\text{gas})] + nE[S(\text{gas})] - E[M_mS_n(\text{gas})] \quad (1)$$

where E[X(gas)] denotes the energy of species X in the gas phase. Table 1 lists E_a(gas) for these gas-phase complexes from PW DFT calculations. These results show that for complexes with more than one metal atom ($m > 1$), the atomization energy is the lowest for Ag and higher for Au and Cu. This correlates with the bulk cohesive energies, E_c^M, of the metals (theoretical values for which are reported below). The atomization energy also generally increases as the size of the complex increases, the main exception being that M_4S_4 (rather than M_4S_5) has the largest atomization energy among all configurations.

Table 1 also lists the atomization energies using the hybrid PBE0, meta-GGA SCAN,[33] and optB88-vdW functionals. The PBE0 atomization energies are consistently lower than the corresponding PBE values. This trend has been found before, for example, for the G2-1 test set,[47,48] and inclusion of coinage metals here conforms with this trend. On the other hand, the differences between PBE and SCAN values are rather small, with SCAN values being slightly smaller, but with some exceptions. Also note that the trigonal AuS_3 configuration is not (locally) stable for either PBE0 or SCAN functionals. Results using optB88-vdW are almost identical to those from PBE, indicating that dispersion interactions are not significant for these gas-phase complexes.

The atomization energies for diatomic MS can be compared with available experimental values: 2.80 eV for CuS, 2.21 eV for AgS, and 2.59 eV for AuS.[49] All functionals reproduce the experimental sequence of Cu > Au > Ag, with PBE0 closest to experimental values. However, one should not assess the validity of a functional based solely on its prediction for the energy of a diatomic bond.

We also calculate the atomization energies for a subset of the above large set of gas-phase complexes using atomic or GTO basis sets. This subset is selected to include all smaller complexes which likely exist on surfaces. Results with three different basis sets (as described in detail in Section 2), and with the PBE and PBE0 functionals, are listed in Table 2. The values using double-zeta basis sets for metals (DZ/TZ) are significantly lower than the two larger basis sets (TZ/TZ and QZ/QZ). With the PBE functional, results using the largest basis set (QZ/QZ) are in excellent agreement with PW-DFT results listed in Table 1. The agreement between PW-DFT and the GTO-DFT is slightly less satisfactory for the PBE0 functional. However, the trend that PBE0 atomization energies are lower than the PBE atomization energies occurs in both GTO and PW sets of calculations.

Next, we comment on the stability of gas-phase complexes based upon the above atomization energies. Because all these energies are positive, the complexes are stable against complete fragmentation into atomic constituents. However, because E_a(gas) is always lower for M_4S_5 than for M_4S_4, this means that the former is thermodynamically unstable against detachment of an S. In contrast, we note that M_4S_5 is stable against fragmentation into M_2S_2 and M_2S_3 and also usually against fragmentation into MS_2 and M_3S_3 (so that instead detachment of an S from M_4S_5 is always favored). By comparing relevant energies, we also find that M_4S_4 is stable against fragmentation into two M_2S_2 or into MS and M_3S_3; M_3S_4 is stable against detachment of an S (discounting PBE0 Ag results) and against fragmentation into MS and M_2S_3 or into MS_2 and M_3S_2; M_2S_3 is stable against fragmentation into MS and MS_2. Therefore, generally, complexes are stable (except M_4S_5). A complete

Table 2. Atomization Energy E_a(Gas) (in Electronvolt) of the Gas-Phase M_mS_n Complex, Obtained Using the NWChem Code with Three Different Basis Sets[a]

		MS_2	MS_3	M_2S_3	M_3S_3	M_3S_4	M_4S_5
Cu				PBE			
	DZ/TZ	5.12	6.97	10.85	15.38	16.10	
	TZ/TZ	5.73	7.65	11.65	16.38	17.02	
	QZ/QZ	5.78	7.70	11.71	16.46	17.10	
	PW	5.82	7.75	11.87	16.63	17.34	22.41
				PBE0			
	DZ/TZ	4.55	5.51	9.28	13.39	13.97	
	TZ/TZ	4.95	6.15	10.01	14.31	14.81	
	QZ/QZ	4.98	6.20	10.08	14.41	14.88	
	PW	5.18	6.17	10.52	15.04	15.47	20.06
Ag				PBE			
	DZ/TZ	4.11	5.22	8.26	11.66	12.25	14.47
	TZ/TZ	4.57	5.90	9.19	12.84	13.49	16.09
	QZ/QZ	4.55	5.96	9.27	12.96	13.60	16.28
	PW	4.52	5.79	9.06	12.69	13.32	17.34
				PBE0			
	DZ/TZ	3.47	3.93	7.10	10.49	10.68	10.51
	TZ/TZ	3.91	4.56	7.92	11.51	11.83	12.28
	QZ/QZ	3.96	4.66	8.01	11.63	11.95	
	PW	3.87	4.25	8.00	11.82	11.57	15.87
Au				PBE			
	DZ/TZ	5.19	6.40	10.13	13.49	14.53	18.81
	TZ/TZ	5.88	7.47	11.33	14.77	16.14	
	QZ/QZ	5.96	7.57	11.48	14.95	16.35	20.73
	PW	5.92	7.51	11.51	14.92	16.41	20.87
				PBE0			
	DZ/TZ	4.41	4.56	8.86	12.02	13.02	14.25
	TZ/TZ	4.94	5.76	9.91	13.36	14.41	16.46
	QZ/QZ	5.00	5.88	10.04	13.55	14.58	16.81
	PW	5.18		10.08	13.56	14.41	18.71

[a]Results from plane-wave VASP analysis (PW) are also included for convenient comparison.

accounting of energy changes for the various fragmentation processes described above is provided in the Supporting Information.

For completeness, we note that it is also common to calculate the formation energy, $E_f(M_mS_n)$(gas), of gas-phase complexes from gas-phase S_2 and bulk metal. This quantity is defined as

$$E_f(M_mS_n)(gas) = E[M_mS_n(gas)] - mE[M(bulk)] - \frac{n}{2}E[S_2(gas)] \quad (2)$$

Here, E[M(bulk)] is the energy per metal atom in the bulk phase and $E[S_2(gas)]$ the energy of the S_2 molecule in the gas phase. Note that here we use S_2 (disulfur) gas as the reference state, even though under standard conditions the most stable phase of sulfur is solid. This definition is partly motivated by the observation that the source of elemental sulfur is predominantly S_2(gas) generated by an electrochemical cell used in many of the experiments.[50] The choice is also partly due to the fact that the solid phase of sulfur is particularly complicated, for example, the orthorhombic α phase has 128 atoms in a single unit cell, such that it poses a significant challenge for computation. That said, it may be more desirable to use a theoretical gas-phase S_8 (*cyclo*-octasulfur) for the reference energy because it is the dominant molecular species for solid sulfur[51] with more S−S bonds than S_2(gas). A comprehensive set of values for E_f(gas) with S_8 as the reference are reported in the Supporting Information. However, these can also be readily obtained by modifying results based upon eq 2 using S_2 as a reference. If one sets $\delta E = E[S_2(gas)]/2 - E[S_8(gas)]/8 = 0.53$ eV (PBE), 0.51 eV (PBE0), 0.48 eV (SCAN), and 0.56 eV (optB88-vdW), then formation energies with the S_8 reference are just $n \times \delta E$ above those with the S_2 reference.

Table 3 lists E_f(gas) values for various gas-phase complexes using different functionals. Note that for the PBE0 functional, we use a screened version (HSE06)[52] to calculate the bulk cohesive energies. The hybrid PBE0 functional generally predicts smaller formation energies than PBE, with the notable exception of MS_3 complexes. In contrast, the meta-GGA SCAN and the optB88-vdW functionals generally predict larger formation energies than PBE. This is mostly due to the larger cohesive energy $E_c^M = E$[M(gas)] − E[M(bulk)] for

Table 3. Formation Energy E_f(Gas) (in Electronvolt) of the Gas-Phase M_mS_n Complex Using the VASP Code[a]

	M	MS	MS_2	M_2S_2	MS_3	M_2S_3	M_3S_3	M_3S_4	M_4S_4	M_4S_5
					PBE					
Cu	3.47	2.73	2.63	1.91	3.20	2.55	1.26	3.04	0.79	3.93
Ag	2.52	2.55	2.99	2.59	4.22	3.46	2.35	4.21	2.57	5.21
Au	3.04	2.59	2.10	2.58	3.01	2.05	1.68	2.68	0.53	3.76
					PBE0					
Cu	2.83	2.25	2.32	1.36	3.68	2.16	0.48	2.39	0.23	2.97
Ag	2.15	2.20	2.93	2.27	4.90	3.30	1.63	4.21	1.47	4.40
Au	2.68	2.39	2.17	2.35		2.29	1.49	2.97	0.58	3.69
					SCAN					
Cu	3.88	3.02	3.13	2.40	3.21	2.84	1.75	3.38	1.29	4.25
Ag	2.90	2.84	3.08	3.21	4.37	3.80	2.81	4.66	3.10	5.77
Au	3.56	2.81	2.13	3.04		1.92	1.72	2.57	0.45	3.44
					optB88-vdW					
Cu	3.53	2.80	2.66	2.13	3.23	2.76	1.56	3.30	1.22	4.16
Ag	2.81	2.82	3.24	3.06	4.33	3.95	3.07	4.89	3.39	6.00
Au	3.41	2.93	2.41	3.20	3.23	2.71	2.60	3.57	1.78	4.92

[a]Note that for M, E_f(gas) is the same as the cohesive energy of the metal. Missing values correspond to unstable complexes.

metals predicted by the latter two functionals, especially for Au.

Although positive values of the gas-phase formation energy do not imply stability in the context of the formation process considered here (i.e., gas-phase complexes are always unstable against incorporation of metal atoms into the bulk and of the S atoms into S_2), lower positive values might be taken as an indicator of stability in other contexts. In this respect, we find that Cu_3S_3, Cu_4S_4, and Au_4S_4 have a particularly strong propensity for stability, with E_f(gas) less than 1 eV at least with some functionals. The MS_2 and M_2S_3 complexes, which have been argued to exist at least on Cu surfaces, do not stand out as particularly stable in this analysis.

3.2. Further Analysis of Energetics and Geometries. To gain further insight into the interactions within the complexes, we also decompose the total interaction energy of the complex into metal−S and metal−metal components, where we focus on the former. Here, we do not explicitly account for any direct sulfur−sulfur interactions as these should be weak, but these are implicitly incorporated into what we identify as M−S interactions. To this end, we define the metal−S binding energy per sulfur atom E_b^{MS}(gas) as

$$E_b^{MS}(\text{gas}) = -\{E[M_mS_n(\text{gas})] - E[M_m(\text{gas})] - nE[S(\text{gas})]\}/n \quad (3)$$

where M_m(gas) is the gas-phase metal cluster obtained by removing all S atoms from the complex. The energy of this metal cluster could be evaluated either with metal atoms frozen in their positions within the equilibrated gas-phase M_mS_n complex (the so-called frozen metal core approach[53]) or with the metal cluster equilibrated. Given $E_a(M_mS_n)$(gas) and E_b^{MS}(gas), the M−M interaction per M atom within the complex follows from E_b^{MS}(gas) via E_b^{MM}(gas) = E[M(gas)] − $E[M_m(\text{gas})]/m$ = $[E_a(M_mS_n)(\text{gas}) - nE_b^{MS}(\text{gas})]/m$.

Results are presented in the Supporting Information for E_b^{MS}(gas) for selected complexes for the frozen core approach, although the basic trends should also be retained for an equilibrated metal cluster. The key observations are as follows: (1) E_b^{MS}(gas) is systematically larger (for all metals) for higher numbers of M per S (i.e., for higher m/n); (2) E_b^{MS}(gas) for $m = n$ increases as n increases; and (3) E_b^{MS}(gas) is typically the largest for Cu, intermediate for Au, and smallest for Ag.

Finally, we comment in more detail on the special case of gas-phase MS_2 complexes, noting that this motif appears to be a common component of stable complexes observed on surfaces. We consider geometry as well as energetics. Figure 2 shows the energy variation for a bent S−M−S complex as a function of angle α = ∠SMS. For all M, the energy initially increases as the angle α deviates from 180° (i.e., as the complex deviates from linear), with Au having the largest energy penalty for bending. Thus, the complex incurs an energy penalty upon bending with S−Au−S being stiffer than S−Cu−S and S−Ag−S. For Cu and Ag, as the angle decreases from 180° to around 120°, the energy starts to drop, and eventually the bent S−M−S complex becomes even more stable than the linear form because of the development of strong S−S bonding. For M = Au, however, this decrease is significantly delayed. As an aside, we remark that while the strongly bent complex has the minimum energy in the gas phase, interaction with the substrate for adsorbed complexes ensures that the linear configuration is the energy minimum.

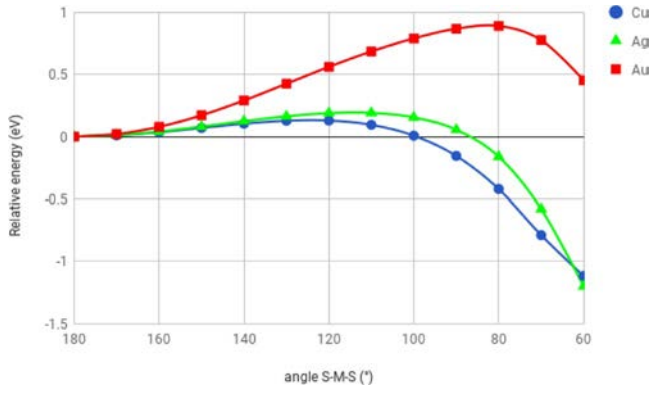

Figure 2. Energy of a bent S−M−S complex in the gas phase as a function of angle α = ∠SMS, where α = 180° for a linear complex. All results are in the same state (A_2) with C_{2v} symmetry and doublet spin multiplicity, using the PBE functional, DZ/TZ basis sets, and the NWChem code.

The propensity for atomic Au to form a linear metal−ligand complex has generally been explained by s−d hybridization[54,55] while that for atomic Cu has been explained by p−d hybridization.[1] This feature is particular to the late transition metals, with filled d shells, while earlier transition metals generally do not possess the propensity for forming the linear S−M−S complexes.[55] From a different perspective, it has long been recognized that chalcogenides of Cu, Ag, and Au generally adopt structures with low metal coordination numbers. This is exemplified by the Cu_2O cuprite ($Pn\bar{3}m$) structure[56] where Cu atoms are linearly coordinated with two oxygen atoms. In contrast, Na_2O (antifluorite, $Fm\bar{3}m$) has Na atoms tetrahedrally coordinated with four O atoms.[57]

4. ENERGETICS OF ADSORBED COMPLEXES

In this section, we explore the energetics of various M_mS_n complexes adsorbed on M(111) surfaces. Calculations are performed with a (4 × 4) supercell which is large enough so that complexes are well separated and do not form direct interconnections. However, for M = Au, analysis with this supercell size does not incorporate the herringbone reconstruction of extended Au(111) surfaces. This is not regarded as a serious shortcoming because exposure of the clean Au(111) surface to S, with possible subsequent formation of complexes, lifts this reconstruction. In general, it is expected that there can be a number of locally stable (or metastable) configurations for adsorbed complexes. While an exhaustive search of the most stable adsorbed structure is complicated, especially for larger m and n, we have reasonable confidence that the lowest energy configurations have been identified.

Figure 3 shows the top views of various M−S complexes determined to be the most stable configuration using DFT-PBE. No stable Au_2S_2 and AuS_3 complexes are found on the Au(111) surface. However, for completeness, we have included dissociated adsorbed structures which result from energy minimization starting with the corresponding gas-phase complexes placed about 0.3 nm above the substrate.

4.1. Surface Atomization Energy of Adsorbed Complexes. Here, we consider the energy to separate adsorbed complexes M_mS_n into isolated M adatoms and chemisorbed S atoms on terraces on the surface

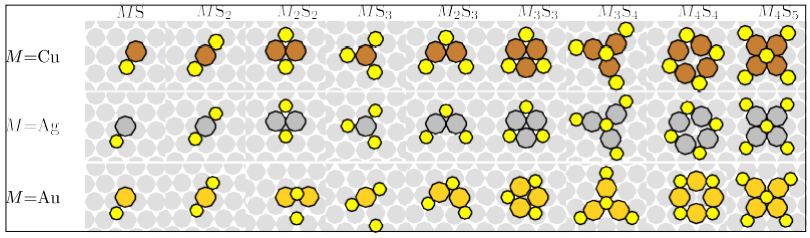

Figure 3. Configurations of the M−S complex adsorbed on the M(111) surface.

Table 4. Surface Atomization Energy, E_a(ads), for Various M_mS_n Complexes Adsorbed on (111) Surfaces, Obtained from VASP Using the PBE Functional[a]

	MS	MS_2	M_2S_2	MS_3	M_2S_3	M_3S_3	M_3S_4	M_4S_4	M_4S_5
Cu(111)	0.11	0.68	0.66	0.66	1.66	2.36	2.48	3.12	3.28
Ag(111)	0.00	0.58	0.36	0.46	1.41	1.97	2.16	2.82	2.96
Au(111)	−0.27	0.12			0.75	1.68	1.83	2.94	2.26

[a]Missing values correspond to unstable complexes.

$$E_a(M_mS_n)(ads) = mE[M(ads)] + nE[S(ads)] - E[M_mS_n(ads)] \quad (4)$$

where E[X(ads)] = E[X(ads + slab)] − E(slab) is the energy of a system with a X adsorbed on the substrate minus the energy of the substrate, with both the clean and adsorbed system optimized independently. We describe this quantity $E_a(M_mS_n)$(ads) as the surface atomization energy because it is the surface analogue of the corresponding gas-phase quantity. A positive value of $E_a(M_mS_n)$(ads) means that the complex is stable against complete fragmentation into separated atomic constituents also residing on a terrace on the surface. To elucidate the relationship between these surface and gas-phase quantities, it is useful to introduce the adsorption energy, E_{ad}(X), of a general species X(ads) through

$$E_{ad}(X) = E[X(ads)] - E[X(gas)] \quad (5)$$

Then by comparing eqs 1 and 4, one can derive a relation for the difference between gas-phase and surface atomization energies of the form

$$E_a(M_mS_n)(ads) - E_a(M_mS_n)(gas) = mE_{ad}(M) + nE_{ad}(S) - E_{ad}(M_mS_n) \quad (6)$$

Ideally, we should obtain the surface atomization energy E_a(ads) in the regime where adsorbed complexes and their dissociated adsorbed constituents sufficiently are far-separated so as to be noninteracting. However, unlike the gas-phase counterpart, there are some complications that make this difficult to do in practice. First, there can be long-ranged interactions between adsorbates mediated by the surface.[58] Elimination of these requires very large supercells in DFT calculations. Second, in the case of Au, isolated adatoms on an extended unreconstructed surface are not stable because the Au(111) surface can spontaneously reconstruct to configurations with a denser first layer. However, we have noted above that exposure to S lifts this reconstruction. Thus, our analysis will correspond to finite coverage, and results will depend slightly on this coverage. Specifically, we evaluate E_a(ads) in eq 4 at a particular coverage of M_mS_n coverage and use E[M(ads)] and E[S(ads)] at the corresponding M and S coverage. For example, using a (4 × 4) supercell, the coverage of the complex is 1/16 ML, the coverage of M is $\theta_M = m/16$ ML, and the coverage of S is $\theta_S = n/16$ ML. We obtain the values at a particular coverage by interpolating results using various supercells.

Table 4 lists the surface atomization energies for the adsorbed complexes shown in Figure 3. Note that for M_3S_3 on M(111), the binding energies for the complexes, which equal $-E_a$(ads), were reported in ref 26. There are some small discrepancies with the current results, the main reason being that the coverage dependence of E[S(ads)] was not considered in ref 26 (specifically, E[S(ads)] was estimated in the limit of zero S coverage).

It is immediately apparent that the atomization energies for adsorbed complexes are much smaller than the corresponding energies for their gas-phase counterparts listed in Tables 1 and 2. This indicates that the intracomplex interactions are much weaker when the complex is adsorbed on the surface, no doubt because of interaction with the metal substrate. Furthermore, while all gas-phase atomization energies are positive, the surface adsorption energy for AuS is negative, indicating that this species is thermodynamically unstable against dissociation into Au and S adatoms adsorbed on the terrace.

In addition, analogous to our discussion of the stability of gas-phase complexes based on atomization energies, one should consider the stability of adsorbed complexes against fragmentation into a small number, for example, two fragment components. A positive E_a(ads), which exceeds the sum of surface atomization energies for various possible fragmentation products, is naturally a prerequisite for stability of the complex on the surface against this incomplete fragmentation process. It is clear that M_4S_5 is always stable against dissociation into M_4S_4 and an adsorbed S, contrary to the analogous gas-phase detachment process. It is also natural to check the stability of M_4S_5 against dissociation into two adsorbed components, MS_2 and M_3S_3, each of which was previously proposed to be a stable surface complex. One finds that M_4S_5 is also stable against such fragmentation (and also against other fragmentation processes). Various incomplete fragmentation pathways for other adsorbed complexes are also unfavorable. A complete accounting of energy changes for various fragmentation processes is provided in the Supporting Information.

However, the above analysis of stability is incomplete as it does not account for the possibility of fragmentation of the complex into chemisorbed S atoms and metal atoms, which are

Table 5. Formation Energy E_f(ads) (in Electronvolt) of Various M_mS_n Complexes on (111) Surfaces, Obtained from VASP Using the PBE Functional

	M	MS	MS_2	M_2S_2	MS_3	M_2S_3	M_3S_3	M_3S_4	M_4S_4	M_4S_5
Cu(111)	0.82	0.66	0.10	0.94	0.11	−0.06	0.11	0.00	0.23	0.08
Ag(111)	0.62	0.59	0.01	0.86	0.13	−0.19	−0.12	−0.31	−0.32	−0.47
Au(111)	0.65	0.81	0.46			0.51	0.29	0.14	−0.24	0.44

incorporated into the substrate at step edges (rather than remaining on terraces on the surface as isolated adatoms). This incorporation process dramatically lowers the system energy, so many complexes with positive E_a(ads) are not stable against this process. A corresponding analysis of stability taking into account the energy cost of extracting adatom from step edges in presented in the next subsection. (Interestingly, this does not require calculating the energies of metal adatoms.)

4.2. Formation Energy of Adsorbed Complexes. We envision the typical pathway for formation of a M_mS_n complex on the surface to involve the following reaction

$$m\mathrm{M(substrate)} + n\mathrm{S(ads)} \xrightarrow{E_f(\mathrm{ads})} \mathrm{M}_m\mathrm{S}_n\mathrm{(ads)} \quad (7)$$

This reaction mechanism reflects the feature that the source of the metal atoms which form the complex is generally expected to be from the substrate, for example, from atoms that are extracted at kink sites along step edges, as clarified further below. On the other hand, the source of S is expected to be from adsorbed atoms on the substrate terraces as also discussed further below. For Ag(111) and Cu(111), step edges are preferred by S over terrace sites, so the above prescription assumes that the S coverage is sufficiently high that step edges are saturated providing excess S atoms on terraces, which can participate in complex formation.

Here, we first discuss the above reaction for general finite temperatures, although our ultimate focus will be on behavior at low T (noting that experiments were performed at 5 K). We describe the change in free energy associated with this reaction as the formation energy, $E_f(M_mS_n)$(ads), of the adsorbed complex. This quantity is obtained from

$$E_f(\mathrm{M}_m\mathrm{S}_n)(\mathrm{ads}) = F(\mathrm{M}_m\mathrm{S}_n + \mathrm{slab}) - F(\mathrm{slab}) - m\mu_M - n\mu_S \quad (8)$$

indicating that the substrate is represented as a slab in our DFT analysis; here, F denotes the free energy and μ_M and μ_S are the chemical potentials of M and S that are the components of the complex, respectively. Negative values of $E_f(M_mS_n)$(ads) imply that the complex is stable against decomposition where S atoms remain on terraces on the surface and metal atoms are reincorporated into the bulk. An advantage in using the free energy in eq 8, rather than just the energy which would generally suffice for low T analysis, is that in this definition there is no ambiguity regarding the choice of the reference energy. Here, we implicitly assume that diffusion of both M and S adatoms is facile so that M adatoms are in equilibrium with the bulk substrate, and sulfur atoms form an equilibrated chemisorbed layer. M−S surface complexes can form naturally through the reaction of S and metal atoms at any of terrace, kink, or step sites. The progressively stronger binding to other metal atoms of metal adatoms which are isolated on terraces, at kink sites along steps, and incorporated at straight close-packed steps means that it is increasingly more energetically expensive to form complexes from such adatoms. This feature is compensated for by the increasing populations of metal atoms at these distinct sites. Thus, the free energy of complex formation is the same no matter where the reaction takes place, again assuming each reactant is in equilibrium and has a well-defined chemical potential.

As indicated above, our focus is on behavior at very low T. As a result, one can clearly ignore vibrational contributions to free energies and chemical potentials. However, it is also necessary to consider the configurational contribution to the free energy of adsorbed layers. In fact, as the coverage of a species approaches zero, this configurational component diverges logarithmically. Thus, even at 5 K, the configurational contribution to the free energy will dominate the energetic component for sufficiently low coverage, thereby destabilizing any complex (even if that complex is stable based on just energetic considerations). Said differently, at sufficiently low coverage, there is a substantial entropic gain from dissociation of the complex. However, as a practical matter, the logarithmic divergence is very slow, and for experimentally relevant coverages, the configurational contribution to the free energy is negligible at 5 K. A quantitative discussion of this issue is provided in the Supporting Information.

For evaluation of μ_M at $T = 0$, it is most straightforward to perform conventional bulk calculations using a unit cell with a single metal atom and periodic boundary conditions. This allows determination of the energy per M atom for an infinite system, so that

$$\mu_M = E[\mathrm{M(bulk)}] = -E_c^M + E[\mathrm{M(gas)}] \quad (9)$$

where E[M(bulk)] is the energy per M atom in the bulk and E[M(gas)] is the energy of an isolated M atom in the gas phase. In practice, because the first two terms in eq 8 are obtained from slab calculations, it is often more accurate to use slab calculations for μ_M to consistently compensate for quantum size effects in the thin slabs.[8,59] We adopt this approach utilizing the same lateral unit cell and M coverage as for the evaluation of surface atomization energy (but where we note that μ_M has a negligible dependence on low coverage).

In typical experiments, both the complexation process and the imaging of adsorbed complexes occur post-deposition rather than under flow conditions. Thus, the relevant parameter controlling the chemical potential, μ_S, of S is the coverage of S on the surface, θ_S. However, the calculation of μ_S is nontrivial. As mentioned earlier, we assume that chemisorbed S adatoms form an equilibrated adlayer. Because of interactions between S adatoms, μ_S is a nontrivial function of the S coverage, even at low temperature. These interactions tend to be repulsive so that there is no clustering of S at low coverages, and μ_S increases with S coverage. To determine the coverage, θ_S, dependence of μ_S, we first calculate the energy of chemisorbed S using various supercells and determine the energy hull by plotting μ_S as a function of $1/\theta_S$.[60] Results for S/Au(111) were given in ref 61 and those for S/Cu(111) and S/Ag(111) were given in ref 62. In evaluating E_f(ads), we utilize interpolated values for μ_S corresponding to the same S

coverage as used for the evaluation of surface atomization energy.

Formation energies for the adsorbed complexes in Figure 3 are summarized in Table 5. We will discuss these results in detail in the following paragraphs. Here, we just note that for (substantial) positive formation energies, the (low) population of such complexes on the surface is given by the corresponding Boltzmann factor. For negative formation energies, all S adsorbed on terraces should be incorporated into such complexes. Note that E_f(ads) reported in Table 5 for Cu−S complexes are slightly lower than the ones cited in ref 1. This is largely due to the lower μ_S value used in ref 1 which is an extrapolation to zero S coverage. As indicated above, here, interpolated values of μ_S at finite S coverages are used. Note that one can readily obtain refined E_f(ads) for any change $\delta\mu_S$ in the chemical potential of S as E_f(ads) just changes by $n\delta\mu_S$.

For S/Cu(111), most adsorbed complexes have small but positive formation energies. However, Cu_2S_3 is stable with a slightly negative formation energy, and other larger complexes such as Cu_3S_4 are marginally stable. This implies that any S on the surface at low temperature would form Cu_2S_3 complexes and/or other larger complexes with negative formation energies. Indeed, STM experiments by Walen et al.[1] at 5 K and very low coverages revealed a heart-shaped complex which was interpreted as the Cu_2S_3 complex. Chainlike concatenations of this complex with stoichiometry Cu_nS_{n+1}, which we denote by $(CuS)_nS$, were observed to develop at least near step edges with increasing S coverage, and DFT calculations with the PBE functional find that these have stabilities close to that of Cu_2S_3 = $(CuS)_2S$, with $E_f((CuS)_3S)$ = 0.02 eV and $E_f((CuS)_4S)$ = 0.01 eV. Other complexes were not seen in experiments.

For S/Ag(111), many complexes have negative formation energies, indicating an enhanced propensity for complexation in this system. Note the general trend of increasingly negative E_f(ads) for larger complexes. Indeed, while earlier STM experiments[63] using liquid nitrogen cooling revealed a dot-row structure with each dot interpreted as a Ag_3S_3 complex, later STM measurements using liquid helium cooling[7] showed more intricate and larger structures, which were interpreted as $Ag_{16}S_{13}$ monomers and $Ag_{13n+3}S_{9n+4}$ chains.

For S/Au(111), the propensity for complexation is limited. Only a ringlike Au_4S_4 complex has a negative E_f(ads) in Table 5. Additional DFT analysis reveals that a similar ringlike Au_6S_6 complex has an even lower E_f(ads) = −0.59 eV. As far as we know, there is no evidence of complexation for S/Au(111) at low coverage. Instead, S adatoms were observed to organize into rows separated from each other by $\sqrt{3}a$ at low S coverage where a denotes the surface lattice constant.[61] Thus, there seems to be a contradiction between experiments and DFT (at least at the GGA level). However, we recall that clean Au(111) undergoes herringbone reconstruction, which, even though lifted by S adsorption, could make theoretical prediction less reliable.

We close this section with some additional comments on complex stability. Certainly, any complex with a negative value of E_f(ads) is stable against dissociation and reincorporation of the metal atoms into the substrate. However, this does not necessarily imply absolute stability. If we define the chemical potential of an S atom in a complex through $\mu_S(M_nS_n) = \{F(M_mS_n + \text{slab}) - F(\text{slab}) - m\mu_M\}/n$, then the complex with the lowest $\mu_S(M_nS_n)$ would be thermodynamically preferred. Note that from eq 8 the difference in chemical potentials of S in a metal−sulfur complex M_mS_n and in an S adlayer can be obtained from the formation energy through $\Delta\mu_S(M_mS_n) = \mu_S(M_mS_n) - \mu_S = E_f(M_mS_n)(\text{ads})/n$. Thus, the formation energy (after dividing by n) provides direct information on the relative and absolute stability of various complexes. For S/Cu(111), the most stable complex is Cu_2S_3, whereas for S/Ag(111), the larger complexes tend to be more stable, consistent with experimental results.

Finally, it is appropriate to comment briefly on situations where the complex has a substantial positive formation energy and where the surface atomization energy is also positive. This applies, for example, for Au_3S_3 with substantial E_f(ads) = 0.29 eV and very high E_a(ads) = 1.68 eV. Thus, while complexes are very stable against fragmentation into atomic constituents, their population on the surface, which is given by $\exp[-E_f(\text{ads})/(k_BT)]$, should actually be low. Thermodynamically, it is preferred for such complexes to dissociate with the Au atoms being incorporated into the Au(111) substrate. However, as noted in the Introduction, one STM study at liquid nitrogen temperatures purported to observe absorbed Au_3S_3 complexes.[4] Recall that S adsorption on Au(111) lifts the herringbone reconstruction, thereby releasing Au atoms onto the terrace. We have argued that such metastable complexes can potentially form because of a supersaturation of Au adatoms associated with lifting of the reconstruction.[26]

5. CONNECTING GAS PHASE AND SURFACE CALCULATIONS

An overall reaction can generally be decomposed into several more elemental steps in multiple ways reflecting multiple distinct pathways. According to Hess's law in thermochemistry, the overall enthalpy change obtained by summing enthalpy changes for the individual steps is independent of the pathway. A standard choice which is convenient for analysis via quantum chemistry calculations is to select isolated gas-phase atoms as the reactants/products for one of the elemental steps. Applying this choice for complex formation on surfaces, one can regard the overall complex formation process as a combination of desorption of atoms from the surface; complex formation in the gas phase; and adsorption of the complex onto the surface

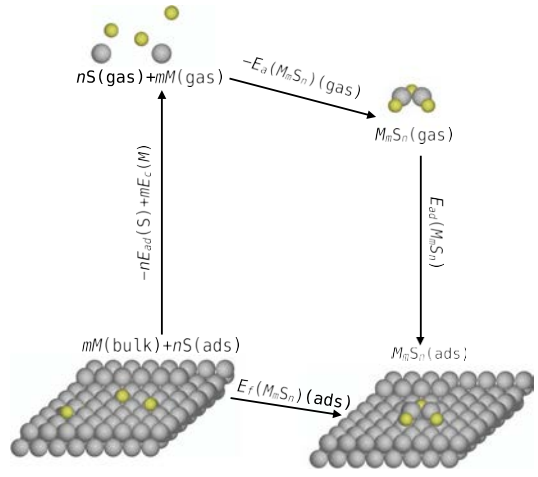

Figure 4. Illustration of the selected pathway and associated energy changes for our analysis of complex formation on surfaces based upon Hess's law. The figure illustrates the specific case of M_2S_3 formation.

Table 6. Adsorption Energy of S and M_mS_n Complex on Various Coinage Metal Surfaces, Obtained Using the PBE functional and the VASP Code[a]

	S	MS	MS_2	M_2S_2	MS_3	M_2S_3	M_3S_3	M_3S_4	M_4S_4	M_4S_5
Cu(111)	−4.40	−3.98	−6.31	−4.74	−8.70	−8.23	−6.77	−10.47	−7.98	−12.82
Ag(111)	−3.64	−3.14	−5.26	−4.01	−7.47	−7.03	−5.85	−8.96	−7.33	−11.17
Au(111)	−3.69	−2.98	−3.92			−4.81	−4.65	−6.74	−4.97	−8.26

[a]Missing values are unstable complexes.

(see Figure 4). Then, schematically, the complex formation process involves the following three steps

$$m\mathrm{M(bulk)} + n\mathrm{S(ads)} \xrightarrow{\Delta E_1} m\mathrm{M(gas)} + n\mathrm{S(gas)}$$

$$\xrightarrow{\Delta E_2} \mathrm{M}_m\mathrm{S}_n\mathrm{(gas)} \xrightarrow{\Delta E_3} \mathrm{M}_m\mathrm{S}_n\mathrm{(ads)} \quad (10)$$

where the energy changes in the different steps are $\Delta E_1 = -nE_{ad}(S) + mE_c(M)$, $\Delta E_2 = -E_a(M_mS_n)(gas)$, and $\Delta E_3 = E_{ad}(M_mS_n)$. Here, $E_{ad}(S)$ and $E_{ad}(M_mS_n)$ are the adsorption energies of the S atom and the M_mS_n complex, respectively. The adsorption process is generally exothermic so that E_{ad} has a negative sign. $E_c(M)$ is the cohesive energy of bulk M, and $E_a(M_mS_n)(gas)$ is the atomization energy of the gas-phase M_mS_n complex, the values of which are given in Table 1. The values of E_{ad} for S and various M−S complexes are given in Table 6.

From Hess's law, one has $E_f = \Delta E_1 + \Delta E_2 + \Delta E_3$. We then tabulate the ΔE_j and E_f for each M−S complex in Table 7 to facilitate analysis. It should be noted that ΔE_3 are the only surface energetics that need to be calculated using DFT separately for each complex. ΔE_1's use the adsorption energy of S, which is the same for all complexes on the same surface, and ΔE_2 is associated with gas-phase processes only. Thus, Table 7 provides a conceptually easy way to connect the adsorption energy and the formation energy of a M−S complex.

Table 7. Decomposition of the Formation Energy of the Metal−Sulfur Complex on Surfaces into Three Elementary Steps[a]

complex	ΔE_1	ΔE_2	ΔE_3	E_f(ads)
CuS	7.88	−3.23	−3.98	0.66
CuS_2	12.23	−5.82	−6.31	0.10
Cu_2S_2	15.70	−10.02	−4.74	0.94
CuS_3	16.57	−7.75	−8.70	0.11
Cu_2S_3	20.04	−11.87	−8.23	−0.06
Cu_3S_3	23.51	−16.63	−6.77	0.11
Cu_3S_4	27.81	−17.34	−10.47	0.00
Cu_4S_4	31.28	−23.06	−7.98	0.23
Cu_4S_5	35.32	−22.41	−12.82	0.08
AgS	6.19	−2.46	−3.14	0.59
AgS_2	9.79	−4.52	−5.26	0.01
Ag_2S_2	12.32	−7.44	−4.01	0.86
AgS_3	13.38	−5.78	−7.47	0.13
Ag_2S_3	15.90	−9.06	−7.03	−0.19
Ag_3S_3	18.43	−12.69	−5.85	−0.12
Ag_3S_4	21.98	−13.32	−8.96	−0.31
Ag_4S_4	24.50	−17.49	−7.33	−0.32
Ag_4S_5	27.81	−17.34	−10.94	−0.47
AuS	6.77	−2.94	−2.98	0.85
AuS_2	10.30	−5.92	−3.92	0.46
Au_2S_2	13.34	−8.49		
AuS_3	13.79	−7.51		
Au_2S_3	16.82	−11.51	−4.81	0.50
Au_3S_3	19.86	−14.92	−4.65	0.29
Au_3S_4	23.29	−16.41	−6.74	0.14
Au_4S_4	26.33	−21.60	−4.97	−0.23
Au_4S_5	29.57	−20.87	−8.26	0.44

[a]Missing values are unstable complexes. The formation energy E_f can be obtained from $E_f = \Delta E_1 + \Delta E_2 + \Delta E_3$.

As is shown in Table 7, step 1 is destabilizing, while steps 2 and 3 are stabilizing. Although systematic trends can be established for each quantity, there seems to be a general compensation effect at work that prevents an easy prediction of E_f(ads). This is not too surprising because a stronger M−S interaction will cause desorption of both individual S atoms and M−S complexes to become more difficult. Also, the atomization energy of M−S in the gas phase is not a reliable indicator of E_f(ads). For example, Cu_3S_3 is much more stable in the gas phase than Cu_2S_3, as measured by E_a or ΔE_2. However, adsorbed Cu_3S_3 is less stable than Cu_2S_3, although only by a small amount. This is due to the significantly smaller $-\Delta E_3$ (i.e., a lower adsorption energy for the complex) and higher $-\Delta E_1$ (associated with a larger cost to extract from the substrate and desorb three vs two Cu atoms) for Cu_3S_3.

The results in Table 7 can be used to provide other insights into complex stability. For example, MS_2 is least stable in the gas phase for M = Ag but most stable as an adsorbed species. This in part reflects the feature that S adsorption on M(111) is weakest for Ag and that extraction of M from the substrate is easiest for Ag. The weak adsorption of AuS_2 also contributes to the low stability of this adsorbed species. Similarly, Ag_2S_3 and Ag_3S_3 are least stable in the gas phase but most stable as adsorbed species. The same factors as above, weak adsorption of S and facile extraction of Ag on Ag(111), contribute to this trend.

6. CONCLUSIONS

We have shown that DFT at the GGA level is quite successful in predicting the stability of adsorbed complexes. For S/Ag(111), Ag_2S_3, Ag_3S_3, Ag_3S_4, Ag_4S_4, Ag_4S_5, and larger complexes are all strongly stable with the S chemical potential generally decreasing for increasing size. For S/Cu(111), Cu_2S_3 is stable, and also, the 3-fold symmetric Cu_3S_4 complex is marginally stable. We have shown that the linear $(CuS)_3S$, $(CuS)_4S$, ..., complexes, which are concatenations of Cu_2S_3, or equivalently of $(CuS)_2S$, have stabilities that are close to that of Cu_2S_3. These results are consistent with STM observations. For S/Au(111), we find that only the ringlike Au_4S_4 is stable. This complex has not been observed in the experiment, but the reliability of the analysis here may be affected by the presence of a surface reconstruction for clean Au(111). Thus, overall, our analysis can be considered quite successful.

This success is perhaps surprising because it is known that DFT prediction of the cohesive energies and atomization energies can suffer from errors as large as 0.5 eV. However,

comparison with extensive STM experiments leads us to believe that DFT prediction of the formation energy is accurate to at least 0.2 eV. The success relies on error cancellations, as indicated by the compensation effects shown in Table 7. All adsorbed M−S complexes with small or negative formation energy incorporate a linear S−M−S motif, with the exception of CuS_3 and AgS_3. This seems to be a feature mainly associated with the d_{10} transition metals, while the nature of ligand (S in this case) has only a secondary effect.[55]

With regard to our analysis of gas-phase complexes, the framework of Hess's law provides a systematic way to relate the results to the stability of adsorbed complexes. In fact, we find that some trends in stability in the gas phase are preserved for adsorbed complexes, while others are not. This reflects the feature that stability on the surface can be regarded within the framework of Hess's law as resulting from a slightly delicate balance between larger energies associated with gas-phase binding within the complex and with adsorption onto the surface.

As noted previously, on both Cu(111) and Ag(111) surfaces, the presence of even trace amounts of S is responsible for a dramatic additive-enhanced acceleration of mass transport. Small 2D homoepitaxial metal islands decay at a rate 2 orders of magnitude higher than on the pristine surface.[9,10] The effective activation barrier for the mass transport pathway associated with a specific mass carrier is given by the sum of the diffusion barrier and the formation energy for the mass carrier (or just the diffusion barrier if the complex formation energy is negative).[8,9,11] This applies irrespective of whether the carrier is a metal adatom or a complex (although for some complexes it is conceivable that there is an additional attachment barrier which must be included). Because the formation energies of metal adatoms are high as indicated in Table 5, even complexes with small positive formation energies (rather than just negative formation energies) can dominate mass transport provided that their diffusion barriers (which are invariably higher than for metal adatoms) are not too high. For development of a detailed kinetic theory for such phenomena, the type of careful and comprehensive assessment of the stability of multiple metal−S complexes on metal(111) surfaces performed in this paper is essential.

ASSOCIATED CONTENT

Supporting Information

The Supporting Information is available free of charge on the ACS Publications website at DOI: 10.1021/acs.jpcc.9b03770.

Coordinates, energies, spin states, and vibrational energies of the gas-phase complexes; spin states for gas-phase complexes; formation energies for gas-phase complexes using octasulfur as a reference; coordinates of the adsorbed complexes with averaging over slab thickness; energy changes for various complex fragmentation processes; assessment of the adlayer configurational contribution to free energy; select molecular orbitals for MS_2; and assessment of M−S interaction strength for gas-phase complexes (PDF)

AUTHOR INFORMATION

Corresponding Author

*E-mail: dajiang@ameslab.gov.

ORCID

Theresa L. Windus: 0000-0001-6065-3167
Patricia A. Thiel: 0000-0003-4195-0216
James W. Evans: 0000-0002-5806-3720
Da-Jiang Liu: 0000-0002-3019-9247

Notes

The authors declare no competing financial interest.

ACKNOWLEDGMENTS

J.L., T.L.W., J.W.E., and D.-J.L. performed the theoretical analysis and computations in this work and were supported by the U.S. Department of Energy (USDOE), Office of Basic Energy Sciences, Division of Chemical Sciences, Geosciences, and Biosciences through the Ames Laboratory Chemical Physics program. The authors acknowledge use of resources of the National Energy Research Scientific Computing Center, a DOE Office of Science User Facility supported by the Office of Science of the U.S. DOE under contract no. DE-AC02-05CH11231. P.A.T. contributed to the formulation of this project and provided experimental insights and was supported for this work by NSF grant no. CHE-1507223. This work was performed at Ames Laboratory, which is operated for the USDOE by Iowa State University under contract no. DE-AC02-07CH11358.

REFERENCES

(1) Walen, H.; Liu, D.-J.; Oh, J.; Lim, H.; Evans, J. W.; Aikens, C. M.; Kim, Y.; Thiel, P. A. Cu_2S_3 complex on Cu(111) as a candidate for mass transport enhancement. *Phys. Rev. B: Condens. Matter Mater. Phys.* 2015, *91*, 045426.

(2) Yamada, M.; Hirashima, H.; Kitada, A.; Izumi, K.-i.; Nakamura, J. Three-Ni-atom cluster formed by sulfur adsorption on Ni(111). *Surf. Sci.* 2008, *602*, 1659−1668.

(3) Kibsgaard, J.; Morgenstern, K.; Lægsgaard, E.; Lauritsen, J. V.; Besenbacher, F. Restructuring of Cobalt Nanoparticles Induced by Formation and Diffusion of Monodisperse Metal-Sulfur Complexes. *Phys. Rev. Lett.* 2008, *100*, 116104.

(4) Kurokawa, S.; Miyawaki, Y.; Sakai, A. Scanning Tunneling Microscopy Observation of Sulfur Adsorbates on Au(111) at Liquid Nitrogen Temperature. *Jpn. J. Appl. Phys.* 2009, *48*, 08JB12.

(5) Wahlström, E.; Ekvall, I.; Kihlgren, T.; Olin, H.; Lindgren, S.-Å.; Walldén L. Low-temperature structure of S/Cu(111). *Phys. Rev. B: Condens. Matter Mater. Phys.* 2001, *64*, 155406.

(6) Walen, H.; Liu, D.-J.; Oh, J.; Lim, H.; Evans, J. W.; Kim, Y.; Thiel, P. A. Reconstruction of steps on the Cu(111) surface induced by sulfur. *J. Chem. Phys.* 2015, *142*, 194711.

(7) Russell, S. M.; Kim, Y.; Liu, D.-J.; Evans, J. W.; Thiel, P. A. Communication: Structure, formation, and equilibration of ensembles of Ag-S complexes on an Ag surface. *J. Chem. Phys.* 2013, *138*, 071101.

(8) Feibelman, P. J. Formation and Diffusion of S-Decorated Cu Clusters on Cu(111). *Phys. Rev. Lett.* 2000, *85*, 606.

(9) Shen, M.; Liu, D.-J.; Jenks, C. J.; Thiel, P. A.; Evans, J. W. Accelerated coarsening of Ag adatom islands on Ag(111) due to trace amounts of S: Mass-transport mediated by Ag-S complexes. *J. Chem. Phys.* 2009, *130*, 094701.

(10) Ling, W. L.; Bartelt, N. C.; Pohl, K.; de la Figuera, J.; Hwang, R. Q.; McCarty, K. F. Enhanced Self-Diffusion on Cu(111) by Trace Amounts of S: Chemical-Reaction-Limited Kinetics. *Phys. Rev. Lett.* 2004, *93*, 166101.

(11) Thiel, P. A.; Shen, M.; Liu, D.-J.; Evans, J. W. Adsorbate-enhanced transport of metals on metal surfaces: Oxygen and sulfur on coinage metals. *J. Vac. Sci. Technol., A* 2010, *28*, 1285.

(12) Wynblatt, P.; Gjostein, N. A. Particle growth in model supported metal catalysts-I. Theory. *Acta Metall.* 1976, *24*, 1165.

(13) Harris, P. J. F. Growth and Structure of Supported metal catalyst particles. *Int. Mater. Rev.* 1995, *40*, 97−115.
(14) Plessow, P. N.; Abild-Pedersen, F. Sintering of Pt Nanoparticle via Volatile PtO_2: Simulation and Comparison with experiments. *ACS Catal.* 2016, *6*, 7098−7108.
(15) Layson, A. R.; Evans, J. W.; Thiel, P. A. Additive-enhanced coarsening and smoothening of metal films: Complex mass-flow dynamics underlying nanostructure evolution. *Phys. Rev. B: Condens. Matter Mater. Phys.* 2002, *65*, 193409.
(16) Kellogg, G. L. Hydrogen promotion of surface self-diffusion on Rh(100) and Rh(311). *Phys. Rev. B: Condens. Matter Mater. Phys.* 1997, *55*, 7206.
(17) Horch, S.; Lorensen, H. T.; Helveg, S.; Lægsgaard, E.; Stensgaard, I.; Jacobsen, K. W.; Nørskov, J. K.; Besenbacher, F. Enhancement of surface self-diffusion of platinum atoms by adsorbed hydrogen. *Nature* 1999, *398*, 134.
(18) Lee, J.; Boschen, J. S.; Windus, T. L.; Thiel, P. A.; Liu, D.-J. Stabilization of X-Au-X complexes on the Au(111) surface: a theoretical investigation and comparision of X=S, Cl, CH_3S, and SiH_3S. *J. Phys. Chem. C* 2017, *121*, 3870−3879.
(19) Stranick, S. J.; Parikh, A. N.; Allara, D. L.; Weiss, P. S. A New Mechanism for Surface Diffusion: Motion of a Substrate-Adsorbate Complex. *J. Phys. Chem.* 1994, *98*, 11136−11142.
(20) Andryushechkin, B. V.; Cherkez, V. V.; Gladchenko, E. V.; Pavlova, T. V.; Zhidomirov, G. M.; Kierren, B.; Didiot, C.; Fagot-Revurat, Y.; Malterre, D.; Eltsov, K. N. Self-organization of Gold Chloride Molecules on Au(111) Surface. *J. Phys. Chem. C* 2013, *117*, 24948−24954.
(21) Parkinson, G. S.; Novotny, Z.; Argentero, G.; Schmid, M.; Pavelec, J.; Kosak, R.; Blaha, P.; Diebold, U. Carbon monoxide-induced adatom sintering in a Pd-Fe_3O_4 model catalyst. *Nat. Mater.* 2013, *12*, 724.
(22) Gerber, T.; Knudsen, J.; Feibelman, P. J.; Grånäs, E.; Stratmann, P.; Schulte, K.; Andersen, J. N.; Michely, T. CO-Induced Smoluchowski Ripening of Pt Cluster Arrays on the Graphene/Ir(111) Moire. *ACS Nano* 2013, *7*, 2020−2031.
(23) Wang, J.; McEntee, M.; Tang, W.; Neurock, M.; Baddorf, A. P.; Maksymovych, P.; Yates, J. T., Jr. Formation, migration, and reactivity of Au-CO complexes on gold surfaces. *J. Am. Chem. Soc.* 2016, *138*, 1518−1526.
(24) Winters, H. F. The etching of Cu(100) with Cl_2. *J. Vac. Sci. Technol., A* 1985, *3*, 786.
(25) Voznyy, O.; Dubowski, J. J.; Yates, J. T., Jr.; Maksymovych, P. The role of Gold adatoms and Stereochemistry in Self-Assembly of Methylthiolate on Au(111). *J. Am. Chem. Soc.* 2009, *131*, 12989−12993.
(26) Liu, D.-J.; Lee, J.; Windus, T. L.; Thiel, P. A.; Evans, J. W. Stability of M_3S_3 complexes on fcc M(111) surfaces: M=Au, Ag, Cu, and Ni. *Surf. Sci.* 2018, *676*, 2−8.
(27) Kresse, G.; Hafner, J. Ab initio molecular dynamics for liquid metals. *Phys. Rev. B: Condens. Matter Mater. Phys.* 1993, *47*, R558−R561.
(28) Kresse, G.; Hafner, J. Ab initiomolecular-dynamics simulation of the liquid-metal-amorphous-semiconductor transition in germanium. *Phys. Rev. B: Condens. Matter Mater. Phys.* 1994, *49*, 14251.
(29) Blöchl, P. E. Projector augmented-wave method. *Phys. Rev. B: Condens. Matter Mater. Phys.* 1994, *50*, 17953.
(30) Kresse, G.; Joubert, D. From ultrasoft pseudopotentials to the projector augmented-wave method. *Phys. Rev. B: Condens. Matter Mater. Phys.* 1999, *59*, 1758−1775.
(31) Perdew, J. P.; Burke, K.; Ernzerhof, M. Generalized Gradient Approximation Made Simple. *Phys. Rev. Lett.* 1996, *77*, 3865−3868.
(32) Adamo, C.; Barone, V. Toward reliable density functional methods without adjustable parameters: The PBE0 model. *J. Chem. Phys.* 1999, *110*, 6158−6170.
(33) Sun, J.; Ruzsinszky, A.; Perdew, J. P. Strongly constrained and appropriately normed semilocal density functional. *Phys. Rev. Lett.* 2015, *115*, 036402.
(34) Klimeš, J.; Bowler, D. R.; Michaelides, A. Chemical accuracy for the van der Waals density functional. *J. Phys.: Condens. Matter* 2010, *22*, 022201.
(35) Klimeš, J.; Bowler, D. R.; Michaelides, A. Van der Waals density functionas applied to solids. *Phys. Rev. B: Condens. Matter Mater. Phys.* 2011, *83*, 195131.
(36) Blöchl, P. E.; Jepsen, O.; Andersen, O. K. Improved tetrahedron method for Brillouin-zone integrations. *Phys. Rev. B: Condens. Matter Mater. Phys.* 1994, *49*, 16223.
(37) Valiev, M.; Bylaska, E. J.; Govind, N.; Kowalski, K.; Straatsma, T. P.; van Dam, H. J. J.; Wang, D.; Nieplocha, J.; Apra, E.; Windus, T. L.; de Jong, W. A. NWChem: a comprehensive and scalable open-source solution for large scale molecular simulations. *Comput. Phys. Commun.* 2010, *181*, 1477−1489.
(38) Hay, P. J.; Wadt, W. R. Ab initio effective core potentials for molecular calculations. Potentials for the transition metal atoms Sc to Hg. *J. Chem. Phys.* 1985, *82*, 270−283.
(39) Wadt, W. R.; Hay, P. J. Ab initio effective core potentials for molecular calculations. Potentials for main group elements Na to Bi. *J. Chem. Phys.* 1985, *82*, 284−298.
(40) Hay, P. J.; Wadt, W. R. *Ab initio* effective core potentials for molecular calculations. Potentials for K to Au including the outermost core orbitals. *J. Chem. Phys.* 1985, *82*, 299−310.
(41) McLean, A. D.; Chandler, G. S. Contracted Gaussian basis sets for molecular calculations. I. Second row atoms, Z=11-18. *J. Chem. Phys.* 1980, *72*, 5639−5648.
(42) Krishnan, R.; Binkley, J. S.; Seeger, R.; Pople, J. A. Self-consistent molecular orbital methods. XX. A basis set for correlated wave functions. *J. Chem. Phys.* 1980, *72*, 650−654.
(43) Clark, T.; Chandrasekhar, J.; Spitznagel, G. n. W.; Schleyer, P. V. R. Efficient diffuse function-augmented basis sets for anion calculations. III. The 3-21+G basis set for first-row elements, Li-F. *J. Comput. Chem.* 1983, *4*, 294−301.
(44) Weigend, F.; Ahlrichs, R. Balanced basis sets of split valence, triple zeta valence and quadruple zeta valence quality for H to Rn: Design and assessment of accuracy. *Phys. Chem. Chem. Phys.* 2005, *7*, 3297.
(45) Andrae, D.; Häußermann, U.; Dolg, M.; Stoll, H.; Preuß, H. Energy-adjusted *ab initio* pseudopotentials for the second and third row transition elements: molecular test for M_2 (M=Ag, Au) and MH (M=Ru, Os). *Theor. Chim. Acta* 1991, *78*, 247−266.
(46) Rappoport, D.; Furche, F. Property-optimized Gaussian basis sets for molecular response calculations. *J. Chem. Phys.* 2010, *133*, 134105.
(47) Curtiss, L. A.; Raghavachari, K.; Redfern, P. C.; Pople, J. A. Assessment of Gaussian-2 and density functional theories for the computation of enthalpies of formation. *J. Chem. Phys.* 1997, *106*, 1063.
(48) Paier, J.; Hirschl, R.; Marsman, M.; Kresse, G. The Perdew-Burke-Ernzerhof exchange-correlation functional applied to the G2-1 test set using a plane-wave basis set. *J. Chem. Phys.* 2005, *122*, 234102.
(49) Huber, K. P.; Herzberg, G. *Molecular Spectra and Molecular Structure IV. Constants of diatomic molecules*; Van Nostrand Reihhold Company: New York, 1979.
(50) Heegemann, W.; Meister, K. H.; Bechtold, E.; Hayek, K. The adsorption of sulfur on the (100) and (111) faces of platinum; a LEED and AES study. *Surf. Sci.* 1975, *49*, 161−180.
(51) Meyer, B. Elemental sulfur. *Chem. Rev.* 1976, *76*, 367.
(52) Krukau, A. V.; Vydrov, O. A.; Izmaylov, A. F.; Scuseria, G. E. Influence of the exchange screening parameter on the performance of screened hybrid functionals. *J. Chem. Phys.* 2006, *125*, 224106.
(53) Larsen, A. H.; Kleis, J.; Thygesen, K. S.; Nørskov, J. K.; Jacobsen, K. W. Electronic shell structure and chemisorption on gold nanoparticles. *Phys. Rev. B: Condens. Matter Mater. Phys.* 2011, *84*, 245429.
(54) Jorgensen, C. K.; Pouradier, J. Un nouveau type de stabilisation du 'champ des ligandes' dans les complexes linéaires du cuivre(I), de l'argent (I) et de l'or (I). *J. Chim. Phys.* 1970, *67*, 124.

(55) Gaudin, E.; Boucher, F.; Evain, M. Some factors governing Ag^+ and Cu^+ low coordination in chalcogenide environments. *J. Solid State Chem.* 2001, *160*, 212−221.
(56) Kirfel, A.; Eichhorn, K. Accurate structure analysis with synchrotron radiation. The electron density in Al_2O_3 and Cu_2O. *Acta Crystallogr., Sect. A: Found. Crystallogr.* 1990, *46*, 271−284.
(57) Evans, R. C. *An Introduction to Crystal Chemistry*, 2nd ed.; Cambridge University Press: Cambridge, 1964.
(58) Einstein, T. L. *Handbook of Surface Science*; Elsevier: Amsterdam, 1996; Vol. *1*: Physical Structure; p 577.
(59) Liu, D.-J. DFT analysis of key energetics in metal homoepitaxy: quantum size effects in periodic slab calculations. *Phys. Rev. B: Condens. Matter Mater. Phys.* 2010, *81*, 035415.
(60) Abufager, P. N.; Zampieri, G.; Reuter, K.; Martiarena, M. L.; Busnengo, H. F. Long-range periodicity of S/Au(111) structures at low and intermediate coverages. *J. Phys. Chem. C* 2014, *118*, 290.
(61) Walen, H.; Liu, D.-J.; Oh, J.; Lim, H.; Evans, J. W.; Kim, Y.; Thiel, P. A. Self-organization of S adatoms on Au(111): $\sqrt{3}$R30° rows at low coverage. *J. Chem. Phys.* 2015, *143*, 014704.
(62) Liu, D.-J.; Thiel, P. A. Oxygen and sulfur adsorption on vicinal surfaces of copper and silver: Preferred adsorption sites. *J. Chem. Phys.* 2018, *148*, 124706.
(63) Shen, M.; Liu, D.-J.; Jenks, C. J.; Thiel, P. A. Novel Self-Organized Structure of a Ag−S Complex on the Ag(111) Surface below Room Temperature. *J. Phys. Chem. C* 2008, *112*, 4281−4290.